Research Article

Experimental Investigation of Heat and Mass Transfer in Tubular Membrane Distillation Module for Desalination

Adnan Al-Hathal Al-Anezi,[1] Adel O. Sharif,[1] M. I. Sanduk,[1] and A. R. Khan[2]

[1] Centre for Osmosis Research and Applications (CORA), Chemical and Process Engineering Department, Faculty of Engineering and Physical Sciences, University of Surrey, Guildford GU2 7XH, UK

[2] Department of Environment Technology and Management, College for Women, Kuwait University, P.O. Box 5969, Safat 13060, Kuwait

Correspondence should be addressed to Adnan Al-Hathal Al-Anezi, AdnanAlHathal@yahoo.com

Membrane distillation is a thermally driven membrane process for seawater desalination and purification at moderate temperatures and pressures. A hydrophobic micro-porous membrane is used in this process, which separates hot and cold water, allowing water vapor to pass through; while restricting the movement of liquid water, due to its hydrophobic nature. This paper provides an experimental investigation of heat and mass transfer in tubular membrane module for water desalination. Different operating parameters have been examined to determine the mass transport mechanism of water vapor. Based on the experimental results, the effects of operating parameters on permeate flux and the heat transfer analysis have been presented and discussed in details.

1. Introduction

Membrane distillation (MD) is a relatively new thermal membrane separation process in which a microporous hydrophobic membrane separates water vapor from a liquid aqueous solution by transport through hydrophobic membrane pores, where the driving force is the vapor pressure difference created by temperature difference across the hydrophobic membrane. The separation mechanism of membrane distillation is based on the principle of vapor-liquid equilibrium [1–3].

Membrane distillation (MD) is attracting increasing desalination research interest because of its low cost. This option saves energy over conventional desalination processes [4]. Importantly, this is considered by most researchers to be a better alternative to traditional desalination processes such as reverse osmosis (RO), multistage flash distillation (MSF), electrodialysis (ED), and so forth. MD produces ultrapure water without high temperatures or high pressures [2].

The aims of this experimental work are to elucidate the mechanism of heat and mass transfers of the MD process, to study the effect of process parameters on permeate flux and to investigate in details the heat transfer process and temperature polarization using a heat-mass transfer analogy.

2. Transport Process

Membrane distillation (MD) is a simultaneous process which involves both heat and mass transfer processes. In MD water vapor, molecules transfer from the warm feed side to the condensation sides. Since both processes are involved the heat and mass transfer profiles are depicted as shown in Figure 1.

2.1. Mass Transfer. The mass transfer of water in MD process generally consists of two steps: the first occurs through the boundary layer at the feed side, and the second occurs across the membrane itself. Mass transfer across the membrane is somewhat complicated and includes several basic mechanisms. There are two approaches for modeling MD. The first one concerns the modeling of the transport mechanism through the hydrophobic membrane. The second concerns with the overall modeling for predicting the permeate flux at given operation conditions [5]. A linear relationship between
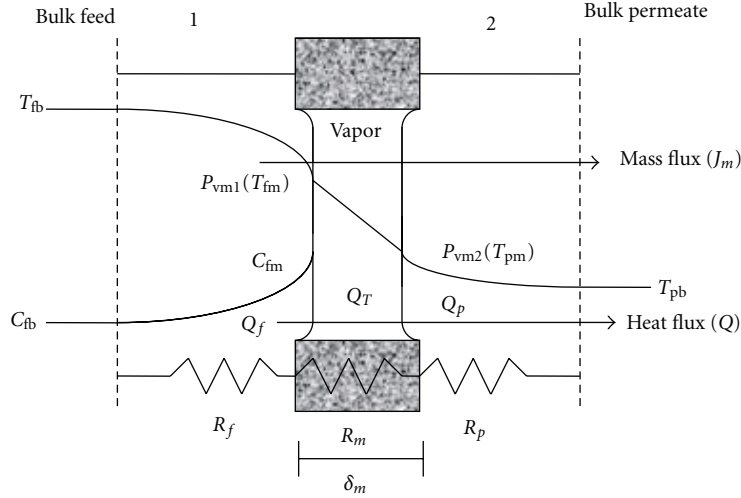
FIGURE 1: Heat and mass transfer profiles in membrane distillation.

the mass flux (J_m) and the water vapor pressure difference ΔP_v across the membrane was suggested to describe the water vapor transport in MD and the basic equation is given by the general expressions [1, 2, 6]:

$$J_m = C_m \Delta P_v = \frac{k_f M_w}{R T_m}(P_{vm1} - P_{vm2}), \qquad (1)$$

where J_m is the water vapor mass flux, C_m is the membrane distillation coefficient and can be a function of pressure, temperature, and the composition within the membrane as well depends on the membrane structure (porosity (ε), thickness (δ_m), pore size diameter (d_p)), k_f is the mass transfer coefficient, and P_{vm1} and P_{vm2} are the vapor pressures of water vapor evaluated at the membrane surface temperatures T_{fm} and T_{pm}. The differences between bulk feed temperatures T_{fb} and T_{fm} and between bulk permeate temperatures T_{pb} and T_{pm} signify the temperature polarization coefficient. The mass transfer coefficient C_m can be determined experimentally or theoretically [6, 7]. For pure liquid, the water vapor pressure at liquid-vapor interface can be calculated using the Antoine equation [2, 6]:

$$P_v = \exp\left(23.1964 - \frac{3816.44}{T_m - 46.13}\right). \qquad (2)$$

2.2. Heat Transfer. The heat transfer in MD process can be summarized in three steps.

(i) Convection from the feed bulk to the vapor-liquid interface at the membrane surface (i.e., the thermal boundary layer at the feed side)

$$Q_f = h_f\left(T_f - T_{fm}\right), \qquad (3)$$

where Q_f (W/m²) and h_f (W/m² K) are the heat flux and heat transfer coefficients at feed side, respectively.

(ii) Evaporation and conduction through the microporous membrane, where the heat flux can be written as

$$Q_v = J_m \Delta H_v,$$
$$Q_c = \frac{k_m}{\delta_m}\left(T_{fm} - T_{pm}\right). \qquad (4)$$

(iii) Convection from the vapor-liquid interface at the membrane surface to the permeate side (i.e., the thermal boundary layer of the permeate side) [6, 8–10]:

$$Q_p = h_p\left(T_{pm} - T_p\right), \qquad (5)$$

where Q_p (W/m²) and h_p (W/m² K) are the heat flux and heat transfer coefficients at permeate side, respectively.

The total heat flux (Q_T), across the membrane, is expressed by the following equation:

$$\begin{aligned}Q_T &= U\Delta T_b \\ &= \left[\frac{1}{h_f} + \frac{1}{h_m + (J_m\Delta H_v)/\left(T_{fm} - T_{pm}\right)} + \frac{1}{h_p}\right]^{-1}\Delta T_b \\ &= Q_v + Q_c,\end{aligned} \qquad (6)$$

where U is the overall heat transfer coefficient, ΔT_b is bulk temperature difference among the feed and permeate sides, ΔH_v is the latent heat of vaporization, respectively.

Under steady state conditions, derived from the heat balance, the heat transfer in the individual compartments of system is represented by the following equation:

$$\begin{aligned}Q &= h_f\left(T_f - T_{fm}\right) \\ &= h_m\left(T_{fm} - T_{pm}\right) + J_m\Delta H_v = h_p\left(T_{pm} - T_p\right).\end{aligned} \qquad (7)$$
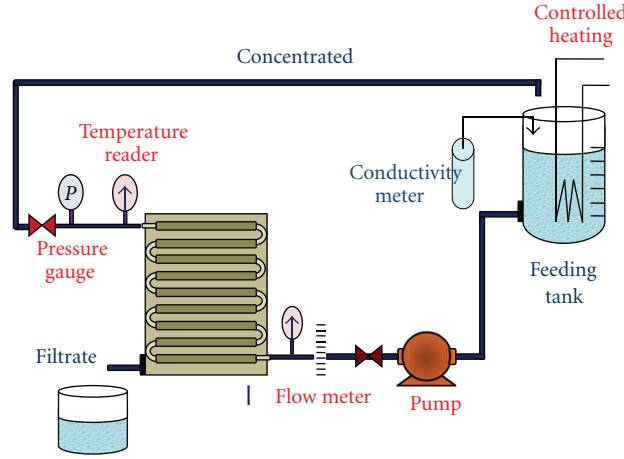
FIGURE 2: Experimental setup.

On the basis of (7), the membrane surface temperatures T_{fm} and T_{pm} on both sides of the membrane can be estimated using the following equations:

$$T_{fm} = \frac{h_m\left(T_p + \left(h_f/h_p\right)T_f\right) + h_f T_f - J_m \Delta H_v}{h_m + h_f\left(1 + h_m/h_p\right)},$$

$$T_{pm} = \frac{h_m\left(T_f + \left(h_p/h_f\right)T_p\right) + h_p T_p + J_m \Delta H_v}{h_m + h_p\left(1 + h_m/h_f\right)}.$$

$$(8)$$

Further the heat transfer coefficient of the membrane h_m can be determined on the basis of thermal conductivities of the membrane k_s and of the vapor that fills the pores k_g, using the following equation:

$$h_m = \frac{k_m}{\delta_m} = \varepsilon \cdot k_s + \frac{(1-\varepsilon)k_g}{\delta_m}. \qquad (9)$$

The heat transfer coefficients of the boundary layers h_f and h_p can be estimated experimentally or can be calculated using empirical correlations of dimensionless groups, namely, Nusselt number (Nu), Reynolds number (Re), and Prandtl number (Pr). These numbers can be calculated directly from the data available for aqueous NaCl solutions and water, using (5) [11–13]:

$$\mathrm{Nu} = a\mathrm{Re}^b\mathrm{Pr}^c, \qquad (10)$$

where a, b, and c are correlation coefficients dependent upon specific hydrodynamic conditions.

2.3. Temperature Polarization. In general, the main resistances are located at the boundary layer within the membrane and also on each side of the membrane.

Boundary layer resistance can be modeled by temperature polarization (TPC). The TPC (Θ) indicates heat transfer boundary layer resistances relative to the total heat transfer resistance

$$\Theta = \frac{\Delta T}{\Delta T_{\max}} = \frac{\left(T_{fm} - T_{pm}\right)}{\left(T_{fb} - T_{pb}\right)}. \qquad (11)$$

Temperature polarization coefficient (TPC) often used as an indirect index of efficiency for the MD process, for most systems, the range of TPC falls between 0.4 and 0.8 and it is close to unity for a well designed system which means that the system fluid dynamics are in good conditions and the process is controlled by mass transfer within the membrane. Where for the value of TPC approaching zero for poorly designed systems, the process is limited by heat transfer through boundary layers [6, 14, 15].

3. Experimental Investigation

3.1. Experimental Modules. The hydrophobic membrane module used in this work was 9 polymeric tubular membranes tubes arranged in a zigzag mode, with 2.8 m length and 0.013 m inner diameter. The total effective area of the module was 0.1144 m². This polymeric membrane has pH ranged from 1.5 to 12 and maximum temperature and pressure of 80°C and 64 bar, respectively. Nitric acid (0.2%) in distilled water can be used for cleaning this membrane at a temperature of 40°C. The membrane had 0.72 micrometer pore size, 51% porosity, and 600 μm thickness.

3.2. Experimental Apparatus. The experimental setup is shown schematically in **Figure 2**, whereas the schematic diagram of tubular membrane module is shown in **Figure 3**. The feed of pure water and brackish water is fed from a transparent feed tank to the tubular membrane module of area 0.1144 m² by a small diaphragm pump. The pressure gauge was placed at the end of the membrane module for circulating the concentrated stream to the feed tank. The level of the feed is to be observed with time to evaluate the evaporation flux. The feed flow was measured using a Rosemount magnetic flow meter ranged from 60 to 240 L/h. Moreover, the feed is to be kept at constant feed temperatures (40, 50, 60, and 70°C) by using a heat exchanger connected to a controlled temperature water bath. The inlet and outlet temperatures were measured using two thermometers probe attached at both sides of the membrane modules.
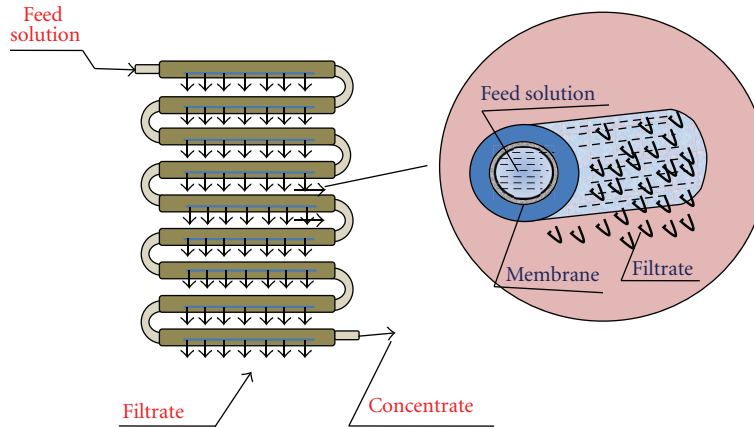
FIGURE 3: Schematic diagram of tubular membrane module.

3.3. Experimental Procedures. For preparing the feed solution, sodium chloride crystals, purchased from Chemical Company, were dissolved in distilled water to produce the required concentration. Brackish sodium chloride solutions were used as a standard saline solution for the investigations. The brackish sodium chloride concentration was measured by conductivity meter. When the experiments were running, the flux measured every 10 minutes, each run lasted for 3 hours. The evaporation flux for each experimental run was the mean value of the fluxes computed at steady state operation with experimental error less than 5%.

4. Results and Discussion

Experiments were carried out using pure water and aqueous solution of sodium chloride NaCl. The effect of operating parameters, namely, feed temperature, feed flow rate, and feed concentration on permeate flux was investigated in these experiments.

4.1. Pure and Saline Water. The first experiments were performed with pure water operated at different feed temperature, the feed bulk temperature values used were 40, 50, 60, and 70°C. During the experiment, the level in the feed tank was observed and maintained by adding the retain amounts of feed water to the feed tank every 10 min. The flux was calculated by plotting the cumulative volume versus time and taking the slope. As shown in **Figure 4**, the experimental flux values have been measured by varying the feed temperature from 40 to 70°C and feed water flow rate from 60 to 240 L/h.

4.2. Membrane Distillation Coefficient and Pure Water Flux. The vapor pressure difference ΔP_{vm} was calculated at the membrane surface temperatures T_{fm} and T_{pm}, and plotted against the steady state fluxes obtained at selected feed temperatures as illustrated in **Figure 5**. On the basis of (1), it can be concluded that the slope of the straight line of the plot thus obtained gives the value of membrane distillation coefficient ($C_m = 0.0004 \, \text{kg/m}^2 \, \text{h Pa}$). The membrane distillation coefficient remains constant for a specific membrane
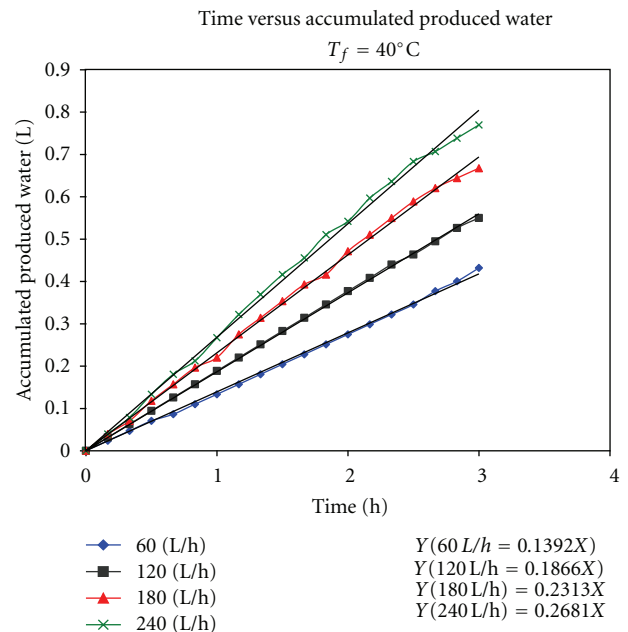

FIGURE 4: Accumulative produced water versus time at feed temperature 40°C.

and vapor properties. Therefore, the membrane distillation coefficient C_m obtained from pure water data can be used to predict the fluxes at different operating conditions.

4.3. Knudsen Number (K_n). Knudsen number K_n can be used as a first criteria for determining the predominant mechanism for water transport through tubular membrane module. K_n is defined as the ratio of the mean free path (λ) of diffusing molecules and the membrane pore diameter (d_p):

$$K_n = \frac{\text{mean free path of water vapor}}{\text{membran pore size}} \implies K_n = \frac{\lambda}{d_p}. \quad (12)$$
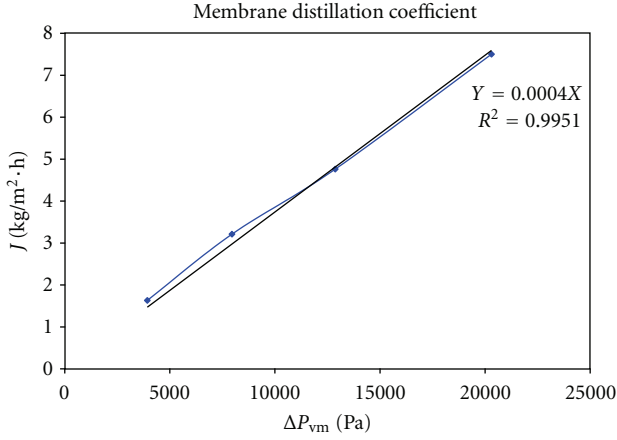
FIGURE 5: Water flux versus ΔP_{vm} at different feed temperatures, feed flow rate 120 L/h; permeate temperature 23°C.
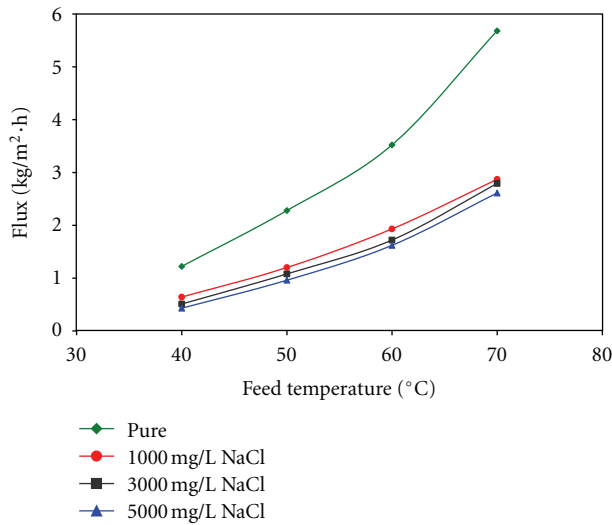

FIGURE 7: Effect of feed flow rate on permeate at feed temperature 70°C and 5000 mg/L of NaCl solution.

FIGURE 6: Effect of feed temperature on permeate flux at constant flow rate 60 L/h and permeate temperature 23°C.
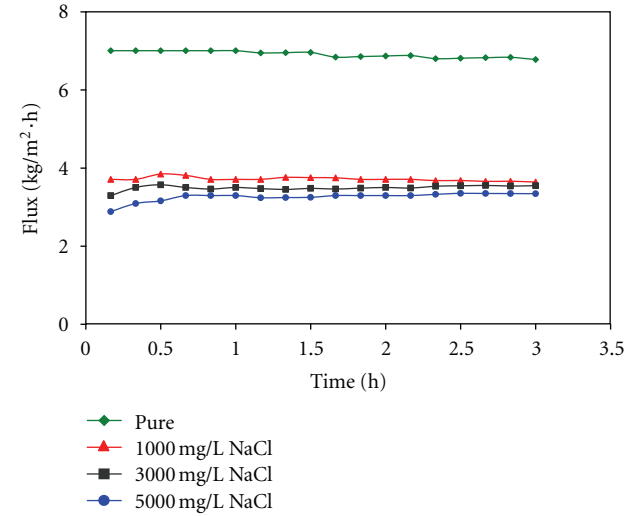
FIGURE 8: Effect of feed concentration on permeate at feed temperature 60°C and at feed flow rate 240 L/h.

According to kinetic theory of gases, the mean free path (λ) can be calculated as follows [16]:

$$\lambda = \frac{3\mu_v}{P}\sqrt{\frac{\pi R T_m}{8 M_w}}.\tag{13}$$

Since K_n was equal to 0.12, the Knudsen-Molecular transition diffusion mechanism regulates the mass transfer within the membrane pores [9].

4.4. Effect of Feed Temperature on Permeate Flux.

Permeate flux is largely dependent on feed temperature. Fluxes of pure water and aqueous NaCl solution are represented in Figure 6. Increasing of feed temperature leads to increase in permeate flux as a consequence of rise in vapor pressure of gas-liquid interface on liquid feed side, which causes a simultaneous increase in the driving force of mass transfer.
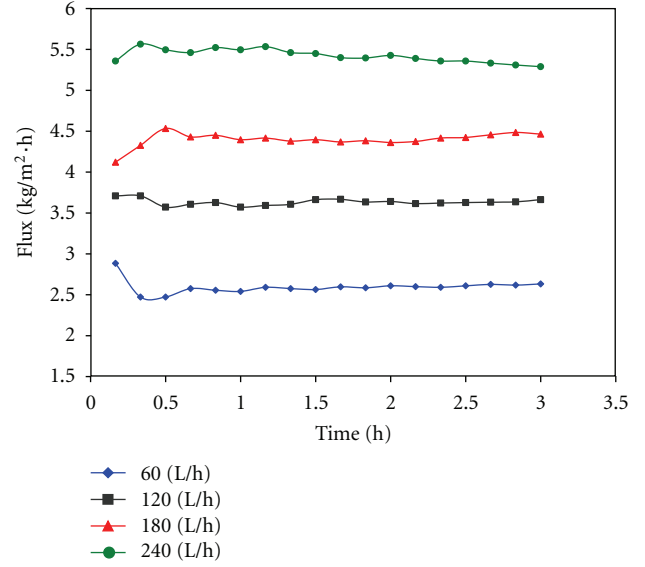
4.5. Effect of Feed Flow Rate on Permeate Flux.

At a constant temperature, the mass flux is dependent on feed flow rateS as depicted in Figure 7 showing the flux time curve at different feed flow rate at a constant temperature of 70°C. The mass flux is directly proportional to feed flow rate since a rise in feed flow rate causes a rise in turbulence, reduction of heat transfer resistance in the boundary layers, and consequential rise in mass transfer coefficient. Moreover, the increase of feed boundary heat transfer coefficient h_f with Reynolds number leadS to further rise in membrane surface temperature T_{fm} and temperature polarization coefficients as depicted in Figure 8. As a result of higher feed surface temperature T_{fm} and lower permeate surface temperature T_{pm} leads to larger driving force resulting in an increasing

TABLE 1: Heat transfer coefficients of the feed boundary layer.

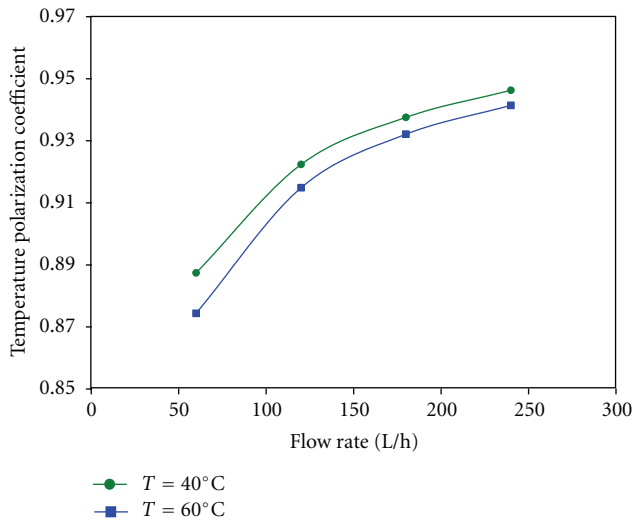| T_f °C	Pure water	Aqueous NaCl, mg/L		
		1000	3000	5000
Re$_f$				
40	7,043	7,438	7,446	7,384
50	8,296	9,123	9,088	9,052
60	9,355	10,259	10,225	10,212
70	10,794	11,015	11,000	10,994
h_f				
40	15,810	9,171	8,714	8,120
50	16,768	9,867	9,459	8,853
60	17,501	10,295	9,944	9,328
70	18,405	10,605	10,283	9,648

FIGURE 9: Temperature polarization coefficients versus feed flow rate at 40 and 60°C feed temperature and 5000 mg/L.

in mass flux. Table 1 lists the examples of heat transfer coefficients.

4.6. Effect of Feed Concentration on Permeate Flux. Feed concentrations are another major factor which affects the permeate flux, where higher concentrations lead to lower permeate flux as shown in Figure 8. Vapor pressure is believed to play an important role of these changes in permeate flux. Decline in permeate flux has also been observed with time, the decrease being further accelerated by increasing feed concentrations. From Figure 9, the feed temperature and the concentrations of aqueous NaCl solution were seen to affect the temperature polarization and concentration polarization on the heat and mass transfer boundary layer thickness. A lowering of vapor pressure as a consequence of rise in concentration of aqueous NaCl solution leads to decline in the driving force across the membrane, thereby causing a lowering of permeate flux.

4.7. Heat Transfer Analysis. On the basis of Figure 9, the values of temperature polarization coefficients can be deduced

to lie within the range of 0.89–0.94 and 0.87–0.93 at 40°C and 60°C feed temperature, respectively. These values are indicative of the suitability of the system design and also portray the fact that mass transfer across the membrane is a major determinant of the process. Increasing in TPC as a consequence of increased feed flow rate is due to lowering of heat transfer resistance within the boundary layer. This leads to an elevation of TPC, which results in increased driving force for mass transfer across the membrane. However, TPC decreased with increase in feed temperature as depicted in Figure 9, and there is an increase in mass flux. However, there is a simultaneous rise in heat flux invading the thermal boundary layer leading to exaggeration of temperature gradient as can be derived from (4) and (7).

Table 2 provides the calculations leading to determination of heat transfer components. Heat flux rises with feed temperatures and falls with feed concentration, which concurs with the above discussion. The resistance across the membrane is approximately 27–46 times larger than that for the feed stream. The loss of conduction across the membrane was 60–85%, which indicated further loss with an increase in feed concentration, but fell with rise in feed temperatures.

5. Conclusions

The experimental flux values of distilled and synthetic salt water have been measured by varying feed temperatures, feed water flow rates, and feed concentration from 40 to 70°C, 60 to 240 (L/h), and 1000 to 5000 mg/L, respectively. The fluxes of distilled and synthetic salt water are related to feed temperatures, feed flow rates, and feed concentrations. The vapor transport mechanism is controlled by Knudsen molecular diffusion transition mechanism depending on temperature, flow rate, and feed concentration. In the present analysis, it is obvious from the results that flux was increased with feed temperatures, feed flow rates and decreased with feed concentrations. The value of membrane distillation coefficient C_m obtained from feed of pure water may be used for predicting the flux. Moreover, it was concluded that the membrane distillation coefficient C_m depends greatly on the operating conditions. The temperature polarization coefficient has been demonstrated to rise with feed flow rate and fall with an increase in feed temperature. TPC values as high as 0.89–0.94 were obtained indicating the efficiency of

TABLE 2: Analysis of heat transfer of the system.

T_f °C	Heat flux, W/m² $Q_f = Q_p = Q_v + Q_c$	U W/m² K	$Q_T = U\Delta T_f$ W/m²	Heat transfer resistance, m² K/W	
				$1/h_f$	$[1/(h_m + (J_m\Delta H_v)/(T_{fm} - T_{pm}))]$
			Pure water		
40	$5,257 = 1,363 + 3,894$	326.50	5,257	6.32×10^{-5}	2.93×10^{-3}
50	$8,766 = 2,713 + 6,053$	348.56	8,766	5.96×10^{-5}	2.75×10^{-3}
60	$11,715 = 3,955 + 7760$	362.12	11,715	5.71×10^{-5}	2.64×10^{-3}
70	$16,260 = 6,327 + 9,933$	390.40	16,260	5.43×10^{-5}	2.45×10^{-3}
			Aqueous NaCl, 1000 mg/L		
40	$4,397 = 715 + 3,682$	282.76	4,397	1.09×10^{-4}	3.32×10^{-3}
50	$7,217 = 1,357 + 5,860$	291.01	7,217	1.01×10^{-4}	3.23×10^{-3}
60	$9,603 = 2,088 + 7,515$	301.03	9,603	9.71×10^{-5}	3.12×10^{-3}
70	$13,028 = 3,418 + 9,610$	317.37	13,028	9.43×10^{-5}	2.96×10^{-3}
			Aqueous NaCl, 3000 mg/L		
40	$4,329 = 648 + 3,681$	277.50	4,329	1.14×10^{-4}	3.37×10^{-3}
50	$7,085 = 1,290 + 5,795$	288.01	7,085	1.06×10^{-4}	3.25×10^{-3}
60	$9,495 = 2,062 + 7,433$	299.99	9,495	1.01×10^{-4}	3.12×10^{-3}
70	$12,801 = 3,345 + 9,456$	316.08	12,801	9.72×10^{-4}	2.96×10^{-3}
			Aqueous NaCl, 5000 mg/L		
40	$4,142 = 560 + 3,582$	271.60	4,142	1.23×10^{-4}	3.42×10^{-3}
50	$6,949 = 1,230 + 5,719$	284.78	6,949	1.13×10^{-4}	3.27×10^{-3}
60	$9,273 = 1,894 + 7,378$	293.90	9,273	1.07×10^{-4}	3.17×10^{-3}
70	$12,330 = 2,952 + 9,377$	305.94	12,330	1.04×10^{-4}	3.05×10^{-3}

system with respect to heat transfer. The heat transfer of the system is controlled by the heat transfer in the membrane where the membrane resistance is 27–46 times higher than that of feed stream.

Nomenclature

C_{fb}: Molar concentration at feed bulk
C_{fm}: Molar concentration at membrane surface
C_m: Mass transfer coefficient (kg/m² h Pa)
M_w: Molecular weight of water (kg/kmol)
d_p: Pore size diameter of the membrane (μm)
ΔH_v: Water vapor latent heat of vaporization (kJ/kg)
h_f: Heat transfer coefficient at the feed side (W/m² K)
h_m: Heat transfer coefficient of the membrane (W/m² K)
h_p: Heat transfer coefficient at the permeate side (W/m² K)
J_m: Mass vapor flux (kg/m² h)
k_f: Mass transfer coefficient (m/s)
k_g: Thermal conductivity of vapor fills the membrane pores (W/m K)
k_m: Average thermal conductivity of membrane and vapor (W/m K)
k_s: Thermal conductivity of the membrane (W/m K)
P: Total pressure (Pa)
P_{vm1}: Water vapor pressure at the feed membrane surface (Pa)

P_{vm2}: Water vapor pressure at the permeate surface (Pa)
ΔP_{vm}: Vapor pressure difference at membrane sides (Pa)
Q_c: Heat flux by conduction (W/m2)
Q_f: Heat flux from the feed bulk to the vapor-liquid interface (W/m²)
Q_p: Heat flux from the vapor-liquid interface to the permeate side (W/m²)
Q_T: Total heat flux (W/m²)
Q_v: Heat flux by vaporization (W/m²)
R: Universal gas constant (m³ Pa/mol K)
R_f: Resistance at feed boundary layer (Pa m² h/kg)
R_m: Resistance at membrane surface (Pa m² h/kg)
R_p: Resistance at permeate boundary layer (Pa m² h/kg)
T_m: Mean temperature (°C, K)
T_f: Water feed temperature (°C, K)
T_{fb}: Temperature at the feed bulk side (°C, K)
T_{pb}: Temperature at the permeate bulk side (°C, K)
T_{fm}: Temperature at the feed membrane surface (°C, K)

T_{pm}: Temperature at the bulk membrane surface (°C, K)
ΔT_b: Bulk temperature difference for feed and permeate sides (°C, K)
U: Overall heat transfer coefficient (W/m² K).

Dimensionless Numbers

K_n: Knudsen number
Re: Reynolds number
Sc: Schmidt number
Sh: Sherwood number
Θ: Temperature polarization coefficient (TPC).

Greek Letters

δ_m: Membrane thickness (m)
ε: Membrane porosity
λ: Mean free path (m).

Subscripts

b: Bulk
Exp.: Experimental
f: Feed
m: Membrane
MD: Membrane distillation
s: Salt
Theor.: Theoretical
w: Water
1: Membrane location at feed side
2: Membrane location at permeate side.

Acknowledgment

References

[1] L. P. Bhausaheb, B. P. Saroj, M. A. Rajendra, and G. Mahendra, "The heat and mass transfer phenomena in vacuum membrane distillation for desalination," *International Journal of Chemical and Biomolecular Engineering*, vol. 3, pp. 33–38, 2010.

[2] J. I. Mengual, M. Khayet, and M. P. Godino, "Heat and mass transfer in vacuum membrane distillation," *International Journal of Heat and Mass Transfer*, vol. 47, no. 4, pp. 865–875, 2004.

[3] S. Al-Obaidani, E. Curcio, F. Macedonio, G. Di Profio, H. Al-Hinai, and E. Drioli, "Potential of membrane distillation in seawater desalination: thermal efficiency, sensitivity study and cost estimation," *Journal of Membrane Science*, vol. 323, no. 1, pp. 85–98, 2008.

[4] M. S. El-Bourawi, Z. Ding, R. Ma, and M. Khayet, "A framework for better understanding membrane distillation separation process," *Journal of Membrane Science*, vol. 285, no. 1-2, pp. 4–29, 2006.

[5] A. Burgoyne and M. M. Vahdati, "Permeate flux modeling of membrane distillation," *Filtration and Separation*, vol. 36, no. 1, pp. 49–53, 1999.

[6] K. W. Lawson and D. R. Lloyd, "Membrane distillation," *Journal of Membrane Science*, vol. 124, no. 1, pp. 1–25, 1997.

[7] L. Martinez-Diez and M. I. Vasquez-Gonsalez, "Effects of polarization on mass transport through hydrophobic porous membranes," *Industrial & Engineering Chemistry Research Journal*, vol. 37, pp. 4128–4135, 1998.

[8] E. Curcio and E. Drioli, "Membrane distillation and related operations—a review," *Separation and Purification Reviews*, vol. 34, no. 1, pp. 35–86, 2005.

[9] L. Zhigang, C. Biaohua, and D. Zhongwei, *Membrane Distillation, Special Distillation Processes*, Elsevier Science, Amsterdam, The Netherlands, 2005.

[10] S. Srisurichan, R. Jiraratananon, and A. G. Fane, "Mass transfer mechanisms and transport resistances in direct contact membrane distillation process," *Journal of Membrane Science*, vol. 277, no. 1-2, pp. 186–194, 2006.

[11] V. Soni, J. Abildskov, G. Jonsson, and R. Gani, "A general model for membrane-based separation processes," *Computers and Chemical Engineering*, vol. 33, no. 3, pp. 644–659, 2009.

[12] T. C. Chen and C. D. Ho, "Immediate assisted solar direct contact membrane distillation in saline water desalination," *Journal of Membrane Science*, vol. 358, no. 1-2, pp. 122–130, 2010.

[13] R. Thanedgunbaworn, R. Jiraratananon, and M. H. Nguyen, "Vapour transport mechanism in osmotic distillation process," *International Journal of Food Engineering*, vol. 5, no. 5, article 3, pp. 1–9, 2009.

[14] A. G. Fane, R. W. Schofield, and C. J. D. Fell, "The Efficient Use of Energy in Membrane Distillation," *Desalination*, vol. 64, pp. 231–243, 1987.

[15] S. Bandini, C. Gostoli, and G. C. Sarti, "Separation efficiency in vacuum membrane distillation," *Journal of Membrane Science*, vol. 73, no. 2-3, pp. 217–229, 1992.

[16] C. Geankoplis, *Transport Processes and Unit Operations*, Prentice-Hall, Englewood Cliffs, NJ, USA, 3rd edition, 1993.